[CANCER RESEARCH 62, 5375–5380, September 15, 2002]

Identifying Microcalcifications in Benign and Malignant Breast Lesions by Probing Differences in Their Chemical Composition Using Raman Spectroscopy[1]

Abigail S. Haka,[2] Karen E. Shafer-Peltier,[3] Maryann Fitzmaurice, Joseph Crowe, Ramachandra R. Dasari, and Michael S. Feld

G. R. Harrison Spectroscopy Laboratory, Massachusetts Institute of Technology, Cambridge, Massachusetts 02139 [A. S. H., K. E. S-P., R. R. D., M. S. F.]; University Hospitals of Cleveland, Case Western Reserve University, Cleveland, Ohio 44106 [M. F.]; and The Cleveland Clinic Foundation, Cleveland, Ohio 44195 [J. C.]

ABSTRACT

We have applied Raman spectroscopy to analyze the chemical composition of microcalcifications occurring in benign and malignant lesions in the human breast. Microcalcifications were initially separated into two categories based on their Raman spectrum: type I, calcium oxalate dihydrate, and type II, calcium hydroxyapatite. Type I microcalcifications were diagnosed as benign, whereas type II were subdivided into benign and malignant categories using principal component analysis, a statistical technique. Although type II microcalcifications are primarily composed of calcium hydroxyapatite, they also contain trace amounts of several biological impurities. Using principal component analysis, we were able to highlight subtle chemical differences in type II microcalcifications that correlate with breast disease. On the basis of these results, we believe that type II microcalcifications formed in benign ducts typically contain a larger amount of calcium carbonate and a smaller amount of protein than those formed in malignant ducts. Using this diagnostic strategy, we were able to distinguish microcalcifications occurring in benign and malignant ducts with a sensitivity of 88% and a specificity of 93%. This is a significant improvement over current X-ray mammography techniques, which are unable to reliably differentiate microcalcifications in benign and malignant breast lesions.

INTRODUCTION

Screening mammography is an important tool in the early detection of breast carcinoma. One feature of particular diagnostic significance is the presence of microcalcifications on the mammogram. Two major types of microcalcifications are found in breast tissue. Type I deposits consist of calcium oxalate dihydrate, a birefringent colorless crystal, whereas type II deposits are composed of calcium phosphates, mainly calcium hydroxyapatite. Type II microcalcifications are typically basophilic on light microscopic examination of H&E stains and nonbirefringent.

There is no reliable way to distinguish between type I and type II microcalcifications in a clinical mammogram, but the type is thought to correlate with disease (1). Calcium oxalate dihydrate crystals are seen most frequently in benign ductal cysts and are rarely found in foci of carcinoma, whereas calcium phosphate deposits are most often seen in proliferative lesions, including carcinoma. This distribution is consistent with the hypothesis that type I microcalcifications are a product of secretions, whereas type II calcium deposits result from cellular degradation or necrosis.

Type II microcalcifications are estimated to occur two to three times more frequently than type I (2). Nonpalpable type II microcalcifications discovered by mammography frequently geographically target the location of the most important abnormality within the breast (3). As such, calcifications are a key component that radiologists look for in a mammogram. Several algorithms have been proposed that attempt to correlate parameters such as the shape, size, number, and roughness of mammographically detected microcalcifications with disease (4–6). However, these studies often exclude cases because of dark mammographic backgrounds, low-density calcific flecks, or densely clustered calcifications, and, thus, are limited to only certain patients and mammograms. To our knowledge, the highest reported sensitivity and specificity for a cross-validated algorithm based on mammography is 71% and 74%, respectively (5). Although these studies show promising results, the diagnosis of breast carcinoma using mammographically detected microcalcifications remains elusive. Whereas the mammographic appearance of microcalcifications bears some relationship to the histological type of the lesion, currently diagnosis cannot be reliably made on this basis.

Because calcium deposits in breast tissue have only been categorized morphologically, significant insight may be gained by examining them using a more rigorous method. Raman spectroscopy is a technique based on the exchange of energy between light and matter. It is an inelastic scattering process in which photons incident on a sample transfer energy to or from the vibrational or rotational modes of a sample. It is a two-photon process and can be thought of as the simultaneous absorption of an incident photon and emission of a Raman photon. The difference between the energies of these two photons corresponds to the transition of a molecule from one energy level to another. Because the energy levels are unique for every molecule, Raman spectra are chemical specific. Individual bands in the Raman spectrum are characteristic of specific molecular motions. Raman spectroscopy is particularly amenable to *in vivo* measurements as the powers and excitation wavelengths used are nondestructive to the tissue (7). Raman spectroscopy is well suited to further the study of microcalcifications in breast tissue, as it can provide a definitive chemical analysis of these morphological structures *in vitro*. In fact, Raman spectroscopy has been used successfully to study calcium deposits in several other organs, such as the kidney and urinary tract (8–13).

In our present study, we have used Raman spectroscopy to highlight differences in the chemical composition or structure of microcalcifications that exist in different lesions in the breast. Results from this study will further our understanding of the chemical changes accompanying the onset and progression of breast disease and provide an important parameter for the diagnosis of breast disease using Raman spectroscopy.

MATERIALS AND METHODS

All of the studies involving human tissue were approved by the University Hospitals of Cleveland and Case Western Reserve University Institutional Review Board, and the Massachusetts Institute of Technology Committee on the Use of Humans as Experimental Subjects.

Tissue Preparation. Raman spectra were acquired from 6-μm thick deparaffinized sections of formalin-fixed, paraffin-embedded breast tissue. Because of their diagnostic importance, microcalcifications in fresh breast tissue cannot

Received 4/25/02; accepted 7/10/02.

The costs of publication of this article were defrayed in part by the payment of page charges. This article must therefore be hereby marked *advertisement* in accordance with 18 U.S.C. Section 1734 solely to indicate this fact.

[1] Supported by Pathology Associates of University Hospitals and NIH Grant P41RR02594.

[2] To whom requests for reprints should be addressed, at G.R. Harrison Spectroscopy Laboratory, Massachusetts Institute of Technology, 77 Massachusetts Avenue, Room 6–014, Cambridge MA 02139.

[3] Present address: Department of Biomedical Engineering, Northwestern University, Evanston, IL 60208.

typically be spared for scientific research, and, thus, our study was confined to examining microcalcifications in fixed tissue sections. Because microcalcifications are relatively inert, the protein cross-linking effects of the fixative should be minimal. Furthermore, Raman spectral line shapes from the calcifications examined in this study are consistent with previously published data acquired from unfixed tissue in other organ systems (8–13). Samples were mounted on MgF_2 flats (Moose Hill Enterprises Inc., Sperryville, VA). Each microcalcification studied was photographed using a phase contrast microscope. The phase contrast images and H&E-stained serial sections were reviewed by an experienced pathologist, who was blinded to the spectroscopy results and rendered a histological diagnosis of the disease state of regions where data were acquired. A total of 30 type I and 60 type II microcalcifications in breast biopsies from 11 patients were examined using Raman spectroscopy, 74 from histologically benign ducts and 16 from histologically malignant ducts. Histological diagnoses for benign ducts ranged from ductal epithelial hyperplasia (3), sclerosing adenosis (19), fibrocystic disease (43), and fibroadenoma (5), to Mönckeberg's arteriosclerosis (4), whereas all 16 of the malignant ducts were diagnosed as DCIS.[4] No invasive carcinomas were encountered in the regions where data were acquired. All 11 of the patients were Caucasian females with a mean age of 53.4 years (range, 41–85 years) and had undergone excisional breast biopsy for suspicious microcalcifications found on mammography. These patients had no palpable breast lesions and, with the exception of the fibroadenomas, had no mass lesion or other significant findings on mammography.

Raman Spectroscopic Measurements. Data were acquired using the Raman microscopy system shown in Fig. 1, which has been described previously (14, 15). In short, Raman excitation light, 830 nm, is launched into a confocal microscope and focused to a spot size of ~2 μm. The objective, 63× (NA 0.9; Zeiss Achroplan), both focuses the excitation and collects the Raman scattered light in a backscattering geometry. A charge coupled device camera atop the microscope allows for registration of the focused laser spot with a white light *trans*-illuminated image. A dichroic beamsplitter and mirror combination redirect the Raman-scattered light to the spectrograph system where it is recorded by a deep-depletion CCD detector (Princeton Instruments, Princeton, NJ) cooled to −110°C. The dispersion of Raman scattered light onto the CCD results in 1.6 cm^{-1} per pixel. All of the Raman spectra in this study were acquired with a 60 s integration time and a spectral resolution of 8 cm^{-1}. The average laser excitation power used varied between 100 and 150 mW.

All of the data processing was preformed in Matlab 5.30. Spectra were Raman shift frequency-calibrated using known spectral lines of toluene. A fifth order polynomial was fit to the spectra by least-square minimization and subsequently subtracted to remove the slowly varying fluorescence background (15). Cosmic rays were removed through the use of a derivative filter.

RESULTS

Raman Spectra. Fig. 2*a* is a specimen radiograph, which exhibits features indicative of the presence of microcalcifications, whereas Fig. 2*b* displays a phase contrast image collected from a thin section of this specimen. The Raman spectrum of a type I microcalcification acquired from the deposit highlighted by a small box in Fig. 2*b* is shown in Fig. 2*c*. On the basis of the overall histology of this sample as well as the specific features apparent in the phase contrast image, this lesion was diagnosed as fibrocystic disease. Vibrational features characteristic of calcium oxalate dihydrate can be seen at 912 cm^{-1}, 1477 cm^{-1}, and 1632 cm^{-1}. These Raman features are attributed to C-C stretching, and C-O symmetric and asymmetric stretching, respectively, and are consistent with previously published Raman spectra of calcium oxalate dihydrate (9, 10, 12).

Fig. 3, *a* and *b* display a phase contrast image of a type II microcalcification in a malignant duct and the corresponding specimen radiograph. Fig. 3*c* shows the Raman spectrum acquired from the deposit highlighted in Fig. 3*a* by a small box. Through examination of this spectrum, it is evident that the microcalcification is not composed of pure calcium hydroxyapatite. The Raman spectrum of pure stoichiometric calcium hydroxyapatite contains four phosphate internal vibrational modes as well as bands because of the hydroxyl ion stretching and librational modes. Two of the phosphate vibrational modes are out of the spectral range we have chosen to examine as well as both of the hydroxyl ion modes. The large band at 960 cm^{-1} is the $\nu_1(PO_4)$ totally symmetric stretching mode of the "free" tetrahedral phosphate ion. Another phosphate ν_1 mode occurs at 948 cm^{-1} but is obscured by the broad phosphate stretching mode at 960 cm^{-1}. Overlapping Raman structure resulting from five $\nu_3(PO_4)$ bands can be seen between 1028 cm^{-1} and 1061 cm^{-1}. The sixth $\nu_3(PO_4)$ mode appears at 1075 cm^{-1}. The phosphate features present are consistent with Raman spectra of calcium hydroxyapatite published previously (8, 11, 13). In addition to the phosphate peaks resulting from calcium hydroxyapatite there are several other vibrational modes present in this spectrum. Protein contributions can be seen at 1445 cm^{-1} and 1650 cm^{-1}. Also the sharp peak present at 1004 cm^{-1} can be attributed to phenylalanine. Small contributions from lipid are manifest as a C-C stretch and C-H (CH_2) bend at 1130 cm^{-1} and 1300 cm^{-1}, respectively.

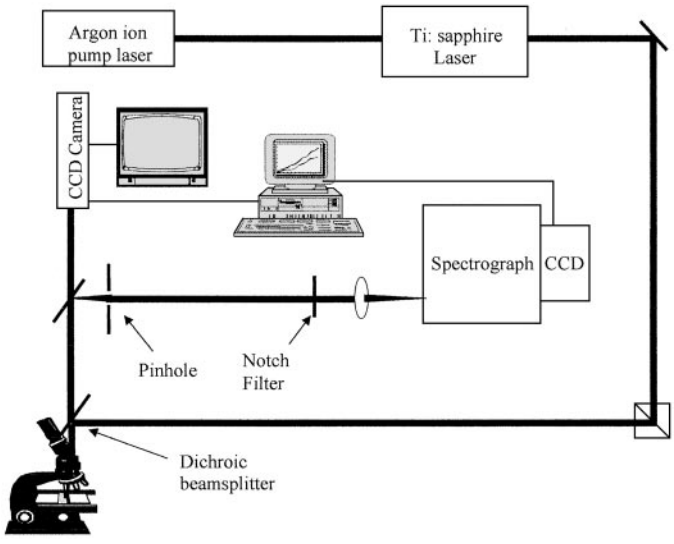

Fig. 1. A schematic representation of the confocal Raman microscopy instrumentation.

Initially, data acquired from type I and type II microcalcifications were separated based on their Raman spectra. The presence or absence of vibrational intensity at specific wavenumbers was used to distinguish between type I and type II microcalcifications. Spectra containing large peaks at 912 cm^{-1} and 1477 cm^{-1}, characteristic of calcium oxalate dihydrate, were grouped into the type I category, whereas spectra displaying intensity at 960 cm^{-1}, characteristic of calcium hydroxyapatite, were grouped into the type II category. In the current analysis, the separation into type I and type II microcalcifications was performed by visual inspection. However, an automated computer algorithm, which normalizes the spectra and distinguishes them based on an intensity value of one occurring at either 960 cm^{-1}, type II, or 1477 cm^{-1}, type I, could easily be implemented. All 30 of the type I microcalcifications we examined were formed in loci of fibrocystic disease and, thus, all 30 of the type I microcalcifications were diagnosed as benign. This is consistent with the fact that type I microcalcifications are formed as a product of secretions and are typically located in cystic lesions. Although type I microcalcifications have been found in malignant lesions, specifically, lobular carcinoma *in situ*, it is exceedingly rare (16, 17).

[4] The abbreviations used are: DCIS, ductal carcinoma *in situ;* PCA, principal component analysis; PC, principal component; FWHM, full width at half maximum; ROC, receiver operating characteristic.

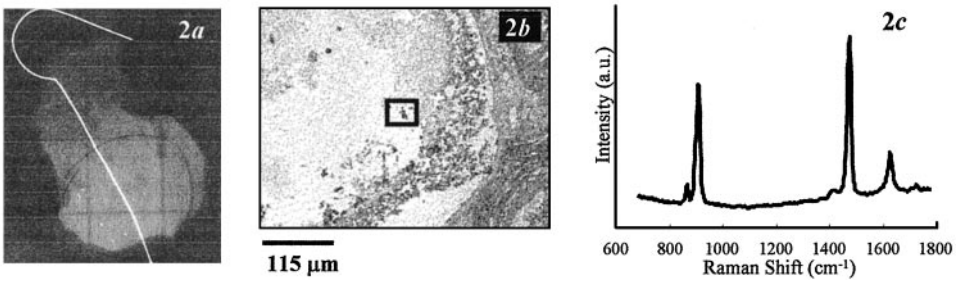

Fig. 2. *a*, specimen radiograph and *b*, phase contrast image taken from a section of the same sample. *c*, Raman spectrum of a type I calcification arising in association with secretions in the lumen of a duct cyst in a focus of fibrocystic disease. The region from which the Raman spectrum was acquired is highlighted by a *box*.

PCA. To differentiate type II microcalcifications occurring in benign and malignant breast lesions, we used a multivariate statistical method of analysis called PCA (18). Similar methods have been used to classify diseased tissue samples in several other organ systems (19–21). PCA uses the entire Raman spectrum and does not assume any knowledge about the chemical composition of the tissue. It is a chemometric technique that resolves the spectra of an entire data set into a few orthogonal PC spectra. These PC spectra can have negative and positive components, and form a complete basis set that accurately describes all of the data (within limitations imposed by noise) if the PCs are multiplied by the proper weighting coefficients. These weighting coefficients, called scores, are analogous to chemical fractions. As a method based on factor analysis/chemometrics, PCA can recognize small spectral variations and, thus, differentiate samples based on similarities (22). This method of analysis is well suited for the examination of type II breast microcalcifications, as they are primarily composed of calcium hydroxyapatite with minute chemical variance because of biological impurities. PCA provides little physical information in and of itself; however, it is adept at isolating spectral trends that correlate with physical information and thereby provides a basis for development of a diagnostic algorithm. Furthermore, by comparing the line shapes of the diagnostic PC spectra with the spectra of pure chemicals, it is possible to ascribe meaning to them. More importantly, this method of analysis provides a proof of principle that there is indeed important diagnostic information contained within the Raman spectra of type II microcalcifications.

We used a singular value decomposition algorithm to determine the PCs of our data set. The data set was normalized to the 960 cm^{-1} peak height to remove any possible intensity biases and subsequently mean centered before performing PCA to remove features common to all of the spectra thereby highlighting spectral variance. All 60 of the spectra could be accurately modeled above the noise level using nine PCs. The first 6 PCs account for >97% of the total variance in the data. Next, we used logistic regression, a discriminate analysis technique, to generate a diagnostic algorithm that was used to classify the breast lesions into benign and malignant categories (23). Logistic regression correlates the weighting coefficients (scores) of the PCs calculated for each Raman spectrum with the diagnostic categories. Diagnoses were provided by a blinded pathologist. A leave one out cross-validation analysis was used to obtain a robust diagnostic algorithm.

Disease Diagnosis. Fibroadenoma is a benign tumor of a completely different lineage than all of the other lesions we have examined (2). It is most closely related to phylloides tumors, the malignant counterpart of which is not carcinoma but cystosarcoma phyllodes, in which the stroma rather than the epithelium is malignant. Furthermore, the clinician typically knows that a breast lesion is in the fibroadenoma/phyllodes tumor family based on physical examination and features other than microcalcification on mammography (24). As these lesions must be surgically excised for treatment, physicians would be unlikely to use a technique like Raman spectroscopy as an adjunct tool for diagnosis of fibroadenoma. For these reasons, we assessed the performance of the algorithm after excluding samples diagnosed as fibroadenoma from our analysis.

Using a combination of PCA and logistic regression, we were able to examine Raman spectral signatures of type II microcalcifications to determine whether or not breast disease diagnosis could be made on this basis. We obtained good diagnostic accuracy with three PC scores. The significant scores are associated with PC_2, PC_3, and PC_5. PC_5 accounts for 1.0% of the total variance in the data, whereas PC_2 and PC_3 account for 8.8% and 5.2%, respectively. Using these three PCs and a leave one out cross-validation method we were able to predict 14 of 16 DCIS and 34 of 39 benign samples correctly. Thus, type II microcalcifications occurring in benign and malignant breast ducts could be distinguished with a sensitivity of 88% and a specificity of 87%. If we retain all of the samples, the sensitivity and specificity are only slightly degraded, maintaining a sensitivity of 88% with a drop in sensitivity to 80%. A graphic representation of the diagnostic algorithm for type II microcalcifications is shown in Fig. 4. To condense the algorithm into a two-dimensional representation, PC_5 and PC_2, which both have higher scores for benign microcalcifications, were added together to form a single axis. On the basis of this algorithm, all of the samples diagnosed as ductal epithelial hyperplasia and sclerosing adenosis, the benign conditions most commonly confused morphologically with carcinoma, were predicted correctly. Four of 5 type II stromal calcifications occurring in fibroadenoma were misdiagnosed, as well as 2 of 4 arterial calcifications in Mön-

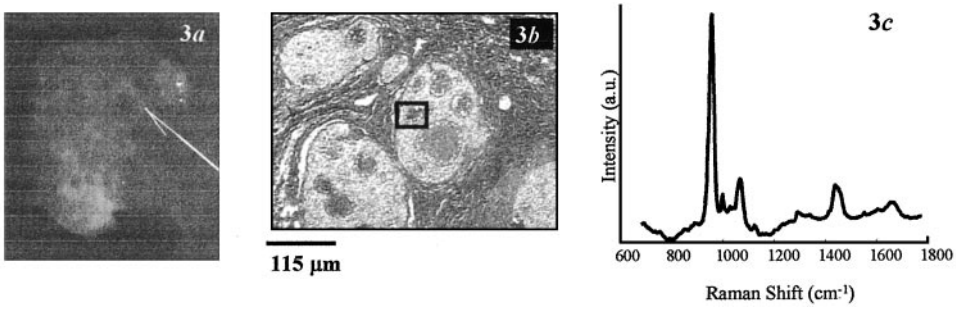

Fig. 3. *a*, specimen radiograph and *b*, phase contrast image taken from a section of the same sample. *c*, Raman spectrum of a type II calcification in a malignant breast lesion. The region from which the Raman spectrum was acquired is highlighted by a *box*.

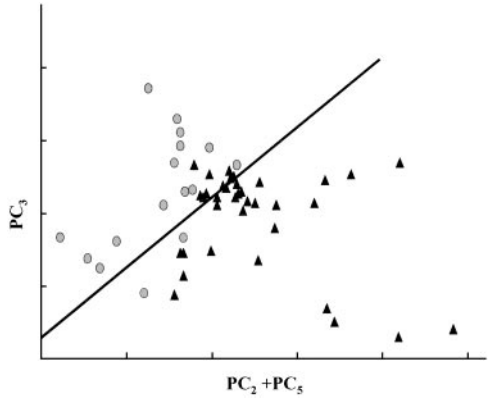

Fig. 4. Diagnostic algorithm for type II microcalcifications based on the scores of three PCs. (▲, benign; ○, malignant).

ckeberg's arteriosclerosis and 3 of 13 ductal calcifications in fibrocystic disease.

In general, only one microcalcification was studied from each lesion. However, in 2 samples, multiple microcalcifications were studied from the same lesion, and no significant differences were seen in the spectra for each given lesion. When we combine data acquired from both type I and type II microcalcifications we obtain an overall sensitivity of 88% and a specificity of 93%. This corresponds to a positive predictive value of 74% and a negative predictive value of 97%. A ROC curve generated from these results is shown in Fig. 5. On the basis of these *in vitro* results in fixed tissue, we believe that Raman spectroscopy has the potential to discriminate microcalcifications associated with benign and malignant breast lesions more accurately than mammography. Additional studies performed *in vitro* on fresh tissue and ultimately *in vivo* are planned to better evaluate the clinical utility of Raman spectroscopy as compared with X-ray mammography for the diagnosis of breast cancer.

Chemical Analysis. Through examination of the three diagnostic PC spectra, we can gain insight into the physical basis responsible for this discrimination. The most diagnostically significant PC spectrum was PC_5, shown in Fig. 6*a*. Examination of this PC spectrum reveals a broadening of the 960 cm^{-1} phosphate stretching peak. This broadening is clearly demonstrated in Fig. 6*b*, in which PC_5 is overlaid with the mean spectrum from all of the type II microcalcifications. Broadening of this peak has been reported in the literature to result from the presence of calcium carbonate (25, 26). In these studies, the application of Raman spectroscopy to carbonated apatite model systems demonstrated a broadening of the phosphate peak with increased carbonate content. The introduction of carbonate ions into the apatite structure reduces the symmetry of its unit cell. The peak broadening results from a loss of long-range translational order in the apatite structure as the carbonate content of the sample increases. The study found a linear relationship between the FWHM of the 960 cm^{-1} phosphate stretching mode and the calcium carbonate content of the sample. Evidence that the broadening at 960 cm^{-1} in PC_5 may result from variations in the calcium carbonate content of the microcalcifications is manifest in a peak at 1070 cm^{-1} attributable to the calcium carbonate $v_1(CO_3)$ mode. However, the difficulty in interpreting PC spectra conferred by the inclusion of both positive and negative features necessitates additional investigation.

If indeed PC_5 accounts for variations in the amount of calcium carbonate present, then spectra that have a higher score for PC_5 will contain a larger amount of calcium carbonate than spectra with a lower weighting coefficient. As benign spectra typically have a larger score for PC_5 than malignant spectra, we postulate that type II microcalcifications occurring in benign lesions of the breast contain a larger amount of calcium carbonate than those deposits found in DCIS. To check our hypothesis, the FWHM was calculated for the 960 cm^{-1} phosphate-stretching peak in each Raman spectrum in our study. In accordance with the theory that type II microcalcifications formed in benign lesions have a larger calcium carbonate content, we found that type II microcalcifications occurring in benign breast lesions had an average FWHM of 18.0 $\pm$ 0.5 cm^{-1}, whereas deposits in lesions diagnosed as DCIS had an average FWHM of 17.0 $\pm$ 0.5 cm^{-1}. The significance of this difference is reflected in a P of 0.03. This value was calculated based on the Wilcoxon rank-sum test, which does not assume a normal distribution of data. Furthermore, if we examine the FWHM of those samples incorrectly diagnosed, we found the opposite trend. The FWHM of benign samples incorrectly diagnosed as malignant was 15.8 $\pm$ 0.5 cm^{-1}, whereas that of malignant samples incorrectly diagnosed as benign was 17.5 $\pm$ 0.5 cm^{-1}, indicating that the width of the phosphate stretching mode is a key diagnostic feature. However, although the peak height of the 1070 cm^{-1} carbonate stretching mode is on average four times larger in benign samples, it does not correlate linearly with the FWHM of the 960 cm^{-1} phosphate-stretching mode. This indicates that additional impurities in the apatite structure contribute to disruption of the symmetry and thereby the broadening of the 960 cm^{-1} peak. These impurities are manifest in the complex vibrational structure of PC_5 but presently have not been identified. PC_5 also contains several features representative of proteins such as the CH_2, CH_3 bending mode at 1445 cm^{-1}, and the Amide I vibration at 1650 cm^{-1}. Unlike the calcium carbonate features, which have a positive intensity, the protein features are negatively directed. This indicates that the protein and carbonate contents are negatively correlated and, thus, that benign samples tend to have a lower protein content than malignant samples.

The amount of protein and calcium carbonate present in type II calcifications in benign and malignant lesions is additionally confirmed by examination of PC_2, shown in Fig. 7. This spectrum also appears to contain positively directed calcium carbonate features, particularly at 1070 cm^{-1}, as well as negatively directed protein features and contributes more, on average, to the Raman spectra of microcalcifications formed in benign ducts. Additionally, PC_2 exhibits a large, second derivative-like feature around 960 cm^{-1}. This type of structure accounts for peak broadening in the data and additionally supports our hypothesis that type II microcalcifications formed in benign ducts tend to have a larger amount of calcium carbonate and,

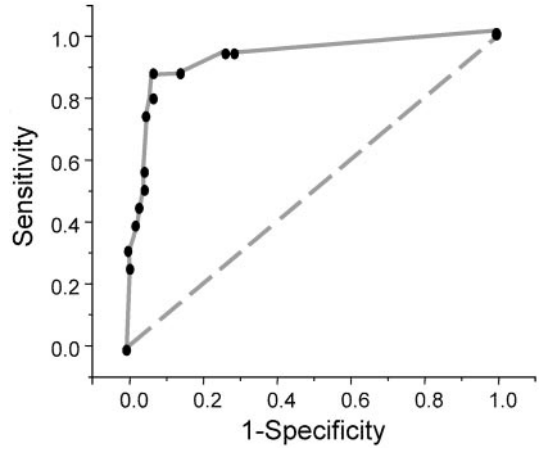

Fig. 5. ROC curve, which illustrates the ability of Raman spectroscopy to separate microcalcifications occurring in benign and malignant breast lesions. A simulated ROC curve of two indistinguishable populations, represented by the *dashed line*, is included for comparison.

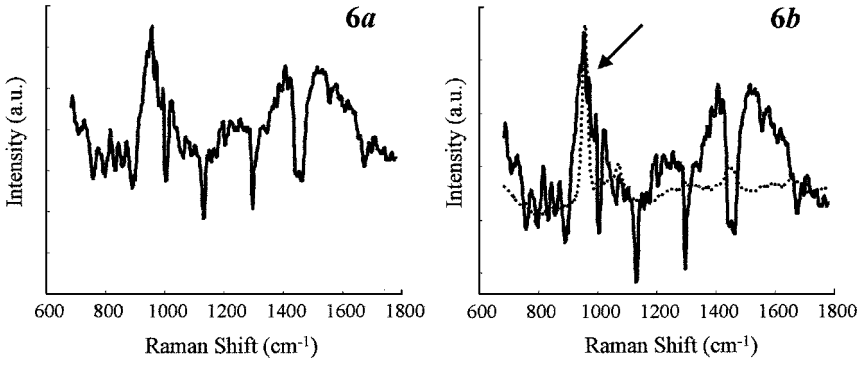

Fig. 6. *a*, PC spectrum 5. *b*, PC spectrum 5 (*solid line*) overlaid with the mean spectrum from all type II microcalcifications (*dotted line*) to illustrate broadening of the 960 cm^{-1} peak (*arrow*).

thus, more broadening of the 960 cm^{-1} peak than those formed in malignant ducts.

PC_3 was also found to be diagnostically significant. It is shown in Fig. 8. However, PC_3 contributes more to Raman spectra acquired from type II calcifications in malignant ducts. It has positively directed protein features, thus lending additional support to the theory that microcalcifications formed in malignant ducts have a larger amount of protein than deposits in benign ducts. The amount of protein in microcalcifications in benign and malignant ducts is confirmed by monitoring the peak height of the Amide I vibration at 1650 cm^{-1}. The intensity of this mode is approximately one and a half times greater in type II microcalcifications formed in malignant lesions. Additionally, contributions from phenylalanine, an amino acid often found in conjunction with collagen and other proteins, can be seen in PC_3 at 1004 cm^{-1}. PC_3 exhibits a large first derivative-like feature at ~960 cm^{-1}. This feature accounts for a peak shift in the phosphate-stretching mode, which is positively correlated with the protein features. The presence of these protein features may explain the misdiagnosis of stromal calcifications in fibroadenomas and arterial calcifications in Mönckeberg's arteriosclerosis, which are the result of stromal or arterial degradation similar to the cellular degradation that occurs in DCIS.

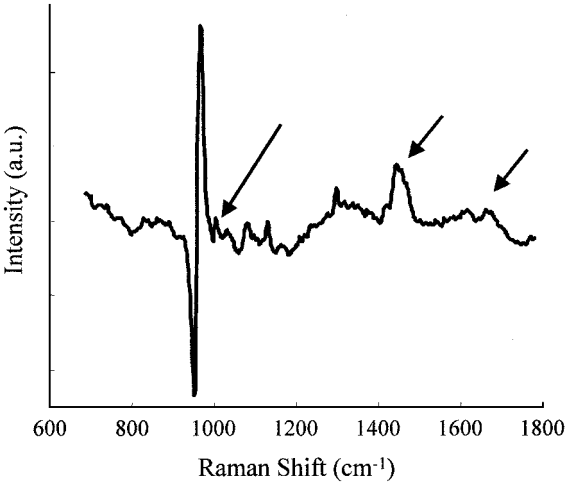

Fig. 8. PC spectrum 3 exhibiting positively directed protein features such as the peak at 1445 cm^{-1}, the Amide I vibration at 1650 cm^{-1}, and the phenylalanine feature at 1004 cm^{-1} (*arrows*).

DISCUSSION

We have demonstrated the diagnostic potential of Raman spectroscopy to differentiate microcalcifications found in benign and malignant breast lesions. Additionally, using PCA we have discovered subtle differences in the chemical composition of type II microcalcifications occurring in benign and malignant breast lesions. On the basis of our results, we postulate that type II microcalcifications occurring in benign lesions of the breast have both a lower protein and a higher calcium carbonate chemical content than those formed in malignant lesions. Although we have identified a few of the chemicals responsible for the differences between benign and malignant type II microcalcifications, there are several other chemical species represented in the rich structural content of the diagnostic PC spectra, which are as yet unidentified. Elucidation of the additional chemical species present in type II breast microcalcifications may yield further insight into the mechanisms by which they are formed.

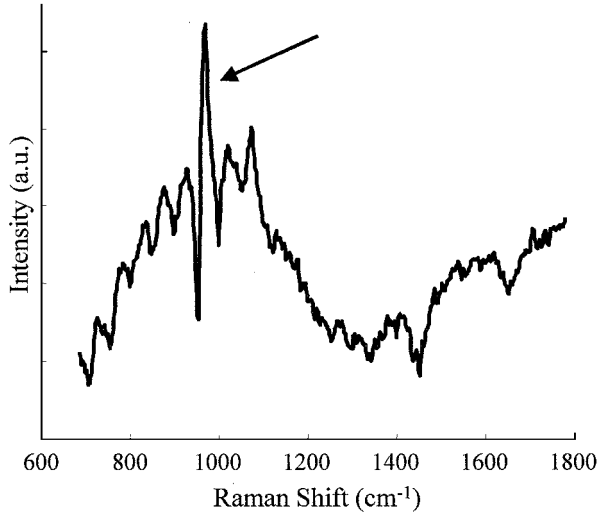

Fig. 7. PC spectrum 2 exhibiting a large, second derivative-like feature around 960 cm^{-1} (*arrow*).

Additional studies are needed to identify these chemical species, and fresh breast tissue may be necessary for these studies. We have found few microcalcifications in the fresh-frozen breast tissue from surgical specimens currently available to us for study because they are important for medical diagnosis and, therefore, not usually released for scientific study. It is for this reason that we used deparaffinized fixed tissue sections for this study. As a result of the fixation process, the fluorescence occurring as a background on the Raman spectrum could not be reliably analyzed. However, the development of fiber-optic probes for Raman spectroscopy may soon allow real-time studies of microcalcifications in fresh breast tissue in the clinical setting before pathologic examination. On the basis of the findings of this study, we expect type II calcifications occurring in benign and malignant lesions to have distinct fluorescent properties because of the known fluorescence characteristics of proteins and calcium carbonate

(27, 28). Additional differences in the fluorescence profile of type II microcalcifications formed in benign and malignant lesions because of as yet unidentified chemical species may also become apparent, once microcalcifications in unfixed tissue are studied. Thus, the fluorescence of type II microcalcifications could easily be exploited to increase the diagnostic accuracy of this methodology. Furthermore, we plan to couple these results with a Raman spectroscopic model of breast tissue described previously to create a powerful new tool for the diagnosis of benign and malignant breast lesions (29). The Raman technique may be applied first *in vitro* in breast biopsies in which little tissue is obtained, and the lesion may not be well represented but microcalcifications are present. Ultimately, it may be used as an *in vivo* adjunct to mammography to help select those patients with microcalcifications who need to go on to biopsy.

REFERENCES

1. Radi, M. J. Calcium oxalate crystals in breast biopsies. Arch. Pathol. Lab Med., *113:* 1367–1369, 1989.
2. Rosen, P. P. Breast Pathology; pp. 143–155. Philadelphia, PA: Lippincott-Raven, 1997.
3. Johnson, J. M., Dalton, R. R., Wester, S. M., Landercasper, J., and Lambert, P. J. Histological correlation of microcalcifications in breast biopsy specimens. Arch. Surg., *134:* 712–716, 1999.
4. Markopoulos, C., Kouskos, E., Koufopoulos, K., Kyriakou, V., and Gogas, J. Use of artificial neural networks (computer analysis) in the diagnosis of microcalcifications on mammography. Eur. J. Radiol., *39:* 60–65, 2001.
5. Betal, D., Roberts, N., and Whitehouse, G. H. Segmentation and numerical analysis of microcalcifications on mammograms using mathematical morphology. Br. J. Radiol., *70:* 903–917, 1997.
6. Shen, L., Rangayyan, R. M., and Desautels, J. E. L. Application of shape-analysis to mammographic calcifications. IEEE T. Med. Imaging, *13:* 263–274, 1994.
7. Hanlon, E. B., Manoharan, R., Koo, T. W., Shafer, K. E., Motz, J. T., Fitzmaurice, M., Kramer, J. R., Itzkan, I., Dasari, R. R., and Feld, M. S. Prospects for *in vivo* Raman spectroscopy. Phys. Med. Biol., *45:* R1–R59, 2000.
8. Kodati, V. R., Tomasi, G. E., Turumin, J. L., and Tu, A. T. Raman spectroscopic identification of phosphate-type kidney stones. Appl. Spectrosc., *45:* 581–583, 1991.
9. Kodati, V. R., Tomasi, G. E., Turumin, J. L., and Tu, A. T. Raman spectroscopic identification of calcium-oxalate-type kidney stone. Appl. Spectrosc., *44:* 1408–1411, 1990.
10. Kontoyannis, C. G., Bouropoulos, N. C., and Koutsoukos, P. G. Use of Raman spectroscopy for the quantitative analysis of calcium oxalate hydrates: application for the analysis of urinary stones. Appl. Spectrosc., *51:* 64–67, 1997.
11. Kontoyannis, C. G., Bouropoulos, N. C., and Koutsoukos, P. G. Raman spectroscopy: a tool for the quantitative analysis of mineral components of solid mixtures. The case of calcium oxalate monohydrate and hydroxyapatite. Vib. Spectrosc., *15:* 53–60, 1997.
12. Pestaner, J. P., Mullick, F. G., Johnson, F. B., and Centeno, J. A. Calcium oxalate crystals in human pathology. Molecular analysis with the laser Raman microprobe. Arch. Pathol. Lab Med., *120:* 537–540, 1996.
13. Kodati, V. R., Tu, A. T., Nath, R., and Turumin, J. L. Analysis of urinary calculi of mixed and unusual composition: Raman spectroscopic investigation. Appl. Spectrosc., *47:* 334–337, 1993.
14. Brennan, J. F., Wang, Y., Dasari, R. R., and Feld, M. S. Near infrared Raman spectrometer systems for human tissue studies. Appl. Spectrosc., *51:* 201–208, 1997.
15. Buschman, H. P., Deinum, G., Motz, J. T., Fitzmaurice, M., Kramer, J. R., van der Laarse, A., Bruschke, A. V., and Feld, M. S. Raman microspectroscopy of human coronary atherosclerosis; biochemical assessment of cellular and extracellular morphologic structures *in situ.* Cardiovasc. Pathol., *10:* 69–82, 2001.
16. Frappart, L., Remy, I., Lin, H. C., Bremond, A., Raudrant, D., Grousson, B., and Vauzelle, J. L. Different types of microcalcifications observed in breast pathology. Correlations with histopathological diagnosis and radiological examination of operative specimens. Virchows Arch. A, *410:* 179–187, 1986.
17. Frappart, L., Boudeulle, M., Boumendil, J., Lin, H. C., Martinon, I., Palayer, C., Mallet-Guy, Y., Raudrant, D., Bremond, A., and Rochet, Y. Structure and composition of microcalcifications in benign and malignant lesions of the breast: study by light microscopy, transmission and scanning electron microscopy, microprobe analysis, and X-ray diffraction. Hum. Pathol., *15:* 880–889, 1984.
18. Geladi, P., and Kowalski, B. R. Partial least-squares regression: a tutorial. Anal. Chim. Acta, *185:* 1–17, 1986.
19. Denium, G., Rodriquez, D., Römer, T. J., Brennan, J. F., Fitzmaurice, M., Myles, J. L., Kramer, J., Lees, R. S., and Feld, M. S. Principal component analysis as a method to correlate the Raman spectrum and the pathology of human coronary artery tissue. Appl. Spectrosc., *53:* 938–942, 1999.
20. Manoharan, R., Shafer, K., Perelman, L., Wu, J., Chen, K., Deinum, G., Fitzmaurice, M., Myles, J., Crowe, J., Dasari, R. R., and Feld, M. S. Raman spectroscopy and fluorescence photon migration for breast cancer diagnosis and imaging. Photochem. Photobiol., *67:* 15–22, 1998.
21. Mahadevan, A., and Richards-Kortum, R. Raman spectroscopy for the detection of cancers and precancers. J. Biomed. Opt., *1:* 31–70, 1996.
22. Brown, S. D. Chemical systems under indirect observation: latent properties and chemometrics. Appl. Spectrosc., *49:* 14A–31A, 1995.
23. Shama S. Applied Multivariate Techniques. New York, NY: John Wiley and Sons, Inc., 1996.
24. Houssami, N., Cheung, M. N., and Dixon, J. M. Fibroademona of the breast. Med. J. Aust., *174:* 185–188, 2001.
25. Nelson, D. G. A., and Williamson, B. E. Low-temperature laser Raman spectroscopy of synthetic carbonated apatites and dental enamel. Aust. J. Chem., *35:* 715–727, 1982.
26. de Mul, F. F. M., Otto, C., Greve, J., Arends, J., and ten Bosch, J. J. Calculation of the Raman line broadening on carbonation in synthetic hydroxyapatite. J. Raman Spectrosc., *19:* 13–21, 1988.
27. Aminzadeh, A. Fluorescence bands in the FT-Raman spectra of some calcium minerals. Spectrochim. Acta A, *53:* 693–697, 1997.
28. Fujimoto, D., Akiba, K., and Nakamura, N. Isolation and characterization of a fluorescent material in bovine achilles tendon collagen. Biochem. Biophys. Res. Commun., *76:* 1124–1129, 1977.
29. Shafer-Peltier, K. E., Haka, A. S., Fitzmaurice, M., Crowe, J., Myles, J., Dasari, R. R., and Feld, M. S. Raman microspectroscopic model of human breast tissue: implications for breast cancer diagnosis *in vivo.* J. Raman Spectrosc., *33:* 552–563, 2002.